High-resolution Ne K Auger spectra from collisions between Ne and H$^+$, Ne^{3+}, Ne^{10+}, Ar^{6+}, and Ar^{16+} (5.5 MeV/u)

I. Kádár, S. Ricz, J. Végh, B. Sulik, D. Varga, and D. Berényi

Institute of Nuclear Research of the Hungarian Academy of Sciences, ATOMKI, H-4001 Debrecen, P.O. Box 51, Hungary

(Received 21 September 1989)

Energetic heavy-ion-impact-induced Ne KLL Auger spectra have been studied by a high-resolution electron spectrometer. To analyze the complex Auger spectra in which many satellite lines are included stemming from multiply ionized neon states, the measured series of interrelated spectra was used with the help of a properly developed computerized procedure. Energy and intensity of the lines in the spectra were determined, and an identification procedure was carried out for all the vacancy configurations from Li-like states to the F-like states (diagram lines). The results were compared with the corresponding theoretical transition energy and intensity values. Based on the above results it was possible to obtain information on the multiple-ionization process at the impact-parameter region of the K-shell ionization. Thus, we have determined the two-dimensional vacancy configuration distribution ($2s,2p$ vacancies) for all the states attainable by Auger transitions. The experimentally determined vacancy configuration distributions did not show any significant difference from the predictions of the independent-particle model. In addition, no definite tendency was found in the ionization probabilities as a function of the degree of ionization.

I. INTRODUCTION

The study of the Auger electrons induced in ion-atom collisions is a very important source of our knowledge concerning collision mechanisms and atomic structure.[1−6] In the 1970s several works of qualitative nature were published on K Auger electron spectra induced by energetic heavy-ion impact.[7,8] These Auger spectra are rather complicated in general and difficult to analyze even if energy resolution of the spectrometer is high and the kinematic effects on the emitted Auger electrons are small, because at energetic ion impact the energy transfer to the target atom is small.[9] The complex structure concerned here is due first of all to the presence of many overlapping satellite lines in these spectra.

The complexity of the K Auger spectra is the probable cause that until recently few works of quantitative character have been published on these spectra dealing with a detailed energy and intensity analysis of them as well as with the identification of the Auger lines. Such a complete analysis of the satellite lines was carried out for the Ne K Auger spectrum at O^{5+} (2.1 MeV/u) impact[10] and regarding the energies for the Ne and N at Xe^{24+} (1.4 MeV/u) impact.[11] There is another possibility to investigate such complex Auger spectra, namely, to study the average quantities characterizing the spectra and the collision process itself.[12,13] In the latter case, however, high-energy resolution is not required.

To overcome the above difficulties arising in the analysis of the spectra in target Auger spectroscopy, the method of the zero-degree Auger spectroscopy[4,14−17] was developed to study the Auger electrons emitted by the outgoing high-energy projectile. High resolution can be achieved by this technique, since the Doppler broadening cancels in first order at zero degree. Zero-degree Auger

spectroscopy has a number of advantages (see, e.g., Ref. 4) in the spectroscopy of highly charged ions. By using light targets (e.g., He) a so-called "needle" ionization (removing mainly one core electron without disturbing the others) takes place and so the Auger spectrum of a projectile ion prepared in a certain charge state can be studied. In this way the spectra are much simpler, the line blending is reduced, and practically the Auger spectrum of the wanted ion species can be studied. At the same time, however, there are some special limitations of this method just in the most advantageous case of the clear needle ionization. From a spectroscopical point of view, only a limited group of ionic states determined by those present in the incident ion beam can be studied. On the other side, Auger lines originating from multiple processes, i.e., containing information about the collision mechanism, usually give only a small part of the spectrum in the needle ionization case. Additionally, some distortions can be present in the intensity ratios because of the alignment and the different lifetimes of the individual states.

To cope with the difficulties concerned we followed another way. Namely, an interrelated series of complex Ne target K Auger spectra of high resolution was taken and evaluated by properly developed computerized procedure. The projectiles are Ne^{3+}, Ne^{10+}, Ar^{6+}, Ar^{16+} (5.5 MeV/u), and also H$^+$ of the same velocity. In the analysis of the spectra, the fact that the transitions originating from different vacancy states (in some cases configurations) are represented in different proportion in the spectra at the impact of different ions, has been used to separate the groups of lines belonging to different initial vacancy states (or configurations). The identification of the Auger lines was also helped eventually by the study of their angular distribution from 0° to 180°. In this way not only energy and intensity values have been deter-

mined for a number of Auger lines but a reliable identification of the lines has been achieved in many cases and then valuable information can be obtained on the collision mechanism and on the decay of the states produced in the collision. Partial results of this study have already been published in recent years.[18−25]

II. EXPERIMENT

The experiments were performed using beams of 5.5 MeV/u H^+, Ne^{3+}, and Ar^{6+} ions provided by the 105-cm cyclotron in ATOMKI, Debrecen (H^+) and the heavy-ion cyclotron U300 in the Joint Institute for Nuclear Research (JINR), Dubna, respectively. The Ne^{10+} and Ar^{16+} beams were produced by stripping the above-mentioned ions by an 80-μg/cm^2-thick carbon foil and selected by the switching magnet of the beamline. The energy of the projectiles has been determined via measuring the energy of the electron loss peak. The projectile current was about 1 μA for H^+ and about 100 nA for the other projectiles. The total counts at the individual spectrum points were produced by several times 10^{12} particles.

The ion beam was strongly collimated to provide an about 2.5-mm-diam ion beam at the target. This strong collimation ensures the free pass of the ion beam through the spherical mirror without touching any of its solid parts.

The electrostatic electron spectrometer used to measure the Ne K Auger spectra consists of a spherical and a double pass, double focusing cylindrical mirror (Fig. 1) designed and built for simultaneous energy and angular distribution measurements[26,27] in ATOMKI, Debrecen. The spherical mirror has a poor (10%) energy resolution. It transports the electrons ejected in the collision from a plane, perpendicular to the axis of the spectrometer and containing the direction of the projectile, to the entrance slit of the vertically directed cylindrical energy analyzer unit. The energy resolution of the spectrometer is determined by the cylindrical mirror. In the present series of measurements it was set to 4.5×10^{-3}. Electrons are detected by 13 channeltrons located at the ring focus of the cylindrical mirror at 13 different angles, including also the 0° and 180° positions. The solid angle of one angular channel is about $4\pi \times 10^{-3}$. The overall energy resolution was improved by using a built-in, spherical decelerating lens located before the entrance slit of the spherical mirror. The spectrometer has been used in a constant pass energy mode at 175-eV cylindrical mirror pass energy, resulting in 1.05 eV full width at half maximum (FWHM) for the 804.5-eV KL_2L_3 ^1D diagram line of neon. The intensity ratio of the spectra taken with and without deceleration was 0.25. This ratio is much higher than that which can be achieved if the energy resolution is improved by narrowing the entrance and exit slits of the cylindrical mirror part of the spectrometer. Further advantage of the constant pass energy mode is that the line shape, the detector efficiency, the transmission of the spectrometer, and the time of flight of the electrons are almost independent of the electron energy.

The gas-beam target was located in the center of the spherical deceleration lens. This very thin target (a few

times 10^{-3} Torr) enabled only single collisions, i.e., the projectile charge state was the same in all collision events. The target pressure was regulated by keeping constant the pressure of a gas buffer before the inlet nozzle (which was constructed from a piece of a channel plate with a 0.2 mm^2 active area).

The calibration of the energy scale was carried out in two steps. The slope was determined by elastic electron scattering, while the intercept by using the energy of the 804.5-eV KL_2L_3 diagram transition measured with high precision by Petterson et al.[28] The energy of the 656.6-eV $1s^12s^12p^1 {}^4P - 1s^2 {}^1S$ transition has been used as a secondary standard in the case of the Ar^{16+}-Ne collision where no diagram line was present. The energy of this secondary standard was determined from the average energy of this transition evaluated from the spectra measured in the Ne^{10+}-Ne and Ar^{6+}-Ne collisions, where both this and the diagram transitions were present.

Matthews et al. have mentioned[10] a broadening of their electron lines due to the charging of their target gas or the Doppler effect. In the present experiments one can expect these effects to be negligible because the impact velocity was higher and the target density was lower than
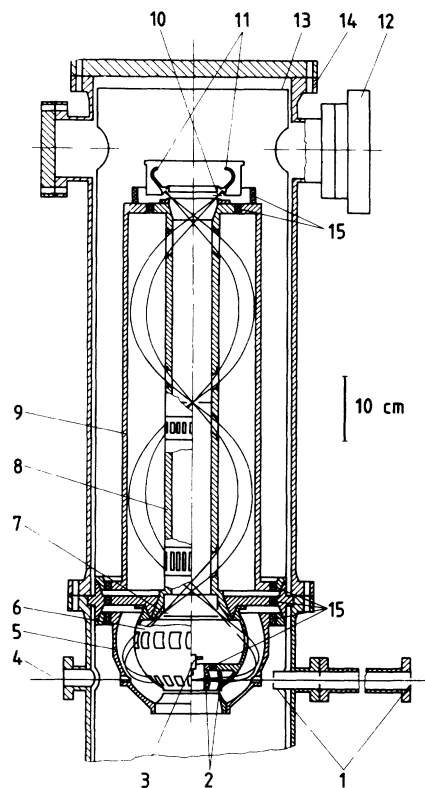

FIG. 1. Schematic cross section of the ESA-21 spectrometer: (1) Collimators, (2) decelerating lens, (3) inlet nozzle of the gas target, (4) Faraday cup, (5) external sphere of the spherical mirror, (6) internal sphere of the spherical mirror, (7) entrance slit of the cylindrical mirror analyzer, (8) internal cylinder of the analyzer, (9) external cylinder of the analyzer, (10) exit slit of the cylindrical mirror analyzer, (11) channel electron multipliers, (12) preamplifiers, (13) magnetic shielding (mumetal), (14) vacuum chamber, (15) ceramic insulators.

in their case. In fact, no target pressure, projectile charge, or projectile mass dependence of either the measured linewidths or the line positions has been found.

For the decomposition of these complex high-resolution K Auger spectra into their components one needs statistically reliable data. The good collimation in the case of a high emittance cyclotron beam implies the consequence that a significant part of the beam intensity is lost on the collimating diaphragms producing background due to nuclear reactions. Since this nuclear background is a source of systematic errors,[29] one should minimize its magnitude and effect. Beside putting the first collimating diaphragm as far from the electron spectrometer as it was possible at all, for further reducing the background the output pulses of the electron detectors were gated by pulses derived from a beam current pickup electrode, thus detecting only those events which occurred at the time of arrival of the beam. This arrangement decreases both the prompt and delayed background intensity due to nuclear reactions using the difference in the time of flight of electrons and gamma rays.[29]

In order to eliminate the eventual long-time instabilities, the spectra have been recorded in several consecutive scans. On the basis of the comparison of these scans a statistical method has been developed[30] to evaluate the eventual systematic error quantitatively. Using this method, we were able to produce statistically reliable spectra with realistic uncertainty.

III. SPECTRUM DECOMPOSITION PROCEDURE

In order to get spectroscopical information on the more or less ionized species of the target atoms, one has to perform a complete decomposition of the spectra, i.e., to determine the energies and intensities of the individual spectrum components by identifying the different satellite and diagram transitions. From the intensity of the identified transitions one can determine the population of the individual ionic levels or configurations by the help of calculated or measured branching ratios. Further, on using the populations obtained in this way one can deduce the cross section of their production and from their relative values the vacancy distribution in the target atom. Even a partial decomposition provides valuable, although not complete information on the above items.

The task to determine the position and intensity of all the peaks present in these complex spectra is not well defined from a mathematical point of view in the case of a single spectrum, since the number of transitions is too large compared to the resolution and the energy range covered by the spectrum. The interrelated spectra of different structure provide the possibility to determine one part of the transitions in one spectrum while getting information for the other part in the next spectrum where these transitions are more expressed (c.f. Fig. 2).

Beside statistically reliable data one needs also realistic line shapes for the decomposition of complex spectra. In the course of the decomposition we found that different line shapes should be used for the metastable and fast decaying transitions. Even the well separable Ne KL_2L_3 diagram line has an asymmetric shape with a tail in its

high-energy side, while the 656.6-eV $1s^12s^12p^14P-1s^2\,^1S$ transition from this metastable Li-like initial state has a symmetric one. This phenomenon can be explained only by a post-collision interaction of the Auger electron with the slow electrons ejected in the collision.[31] The exact solution—the decay-time-dependent line shape—has been approximated by the simpler solution of using two different line shapes, one for the fast and another one (derived from the measured shape of the 656.6-eV metastable transition) for the metastable transitions, not making any further difference inside these two categories.

The full width at half maximum of the peaks has been supposed to be identical for all the peaks, since the post-collision interaction affects essentially only the low intensity part of the lines and the natural linewidth is significantly smaller than the instrumental one.

The post-collision-interaction-affected prompt line shape was calculated according to the model of Niehaus and Zwakhals[32] elaborated for photoelectron emission, using 0.27 eV (Ref. 33) for the natural width of the diagram transition, and an average electron energy of 1200 eV as estimated by a binary encounter approximation (BEA) calculation for the electron spectrum ejected in these collisions. This shape convoluted with an instrumental line shape served as the prompt line shape at the decomposition procedure. Before using it, however, as a first attempt a standard numerical line shape extracted from the measured 804.5-eV KL_2L_3 diagram line was used in the fitting procedure. Introducing the post-collision-interaction (PCI)-affected line shape for the corresponding transitions into the fitting procedure instead of the standard numerical line shape, the normalized χ^2 values fall from 3–5 to 1–2 for all spectra without changing any other parameters.

The minimization program developed for this decomposition is working according to the principle of the least-squares method, i.e.,

$$\chi_n^2 = \frac{1}{f} \sum_{i=1}^{n} W_i [C_i(P) - M_i] \qquad (1)$$

is minimized. Here M_i is the electron intensity measured at energy E_i, C_i is the fitted intensity, calculated with a set of parameters (P), and $W_i = 1/\sigma_i^2$ (σ_i is the uncertainty of M_i). The sum is taken for all points (n) in the spectra and is divided by the number of the degrees of freedom (i.e., n minus the number of the free parameters). The fitted intensity consists of a linear background and the sum of the peaks corresponding to the individual transitions:

$$C_i = B_0 + B_1 E_i + \sum_{k=1}^{N_p} G_k \sum_{m=1}^{N_{p,k}} P_{m,k} I(E_i; E_{m,k}, \sigma) , \qquad (2)$$

where B_0 and B_1 are the coefficients of the linear background, the $N_{p,k}$ peaks due to the transitions from the kth vacancy configuration have a common intensity multiplier G_k. Here σ is the common FWHM of the peaks and $I(E_i; E_{m,k}, \sigma)$ is either of the peak shapes mentioned above. The individual parameters of the peaks are their energy $E_{m,k}$ and their relative intensity $P_{m,k}$. The peaks in group k (corresponding to a certain vacancy

configuration) have a common intensity multiplier, i.e., their absolute intensity is given by $G_k P_{m,k}$. All these parameters can be independently fixed, allowing us to transfer the already known (or supposed tentative) information from one spectrum to another one.

The minimization algorithm is that described by Fletcher[34] based on the variable metric method. The program is capable of handling as many as 200 peaks, with altogether 300 free parameters), a linear background and two different line shapes, so it was able to handle the whole spectrum at the same time.

In practice the following method of analysis has been adopted. At first all spectra excited by different projectiles have been decomposed independently. In regions where no prominent peaks were present, small peaks were added (to fill the gap between the peaks) until no peaklike deviation remained in the residual. In the second step the lines found at the same energy in different spectra were analyzed. Their intensity ratio was found to be grouped according to their initial configuration; see Fig. 6 in Ref. 22. Mainly on this basis peaks in the spectra were assigned to different electron configurations. Then, beginning with the simplest spectra we determined the intensity ratio of different transitions for these groups
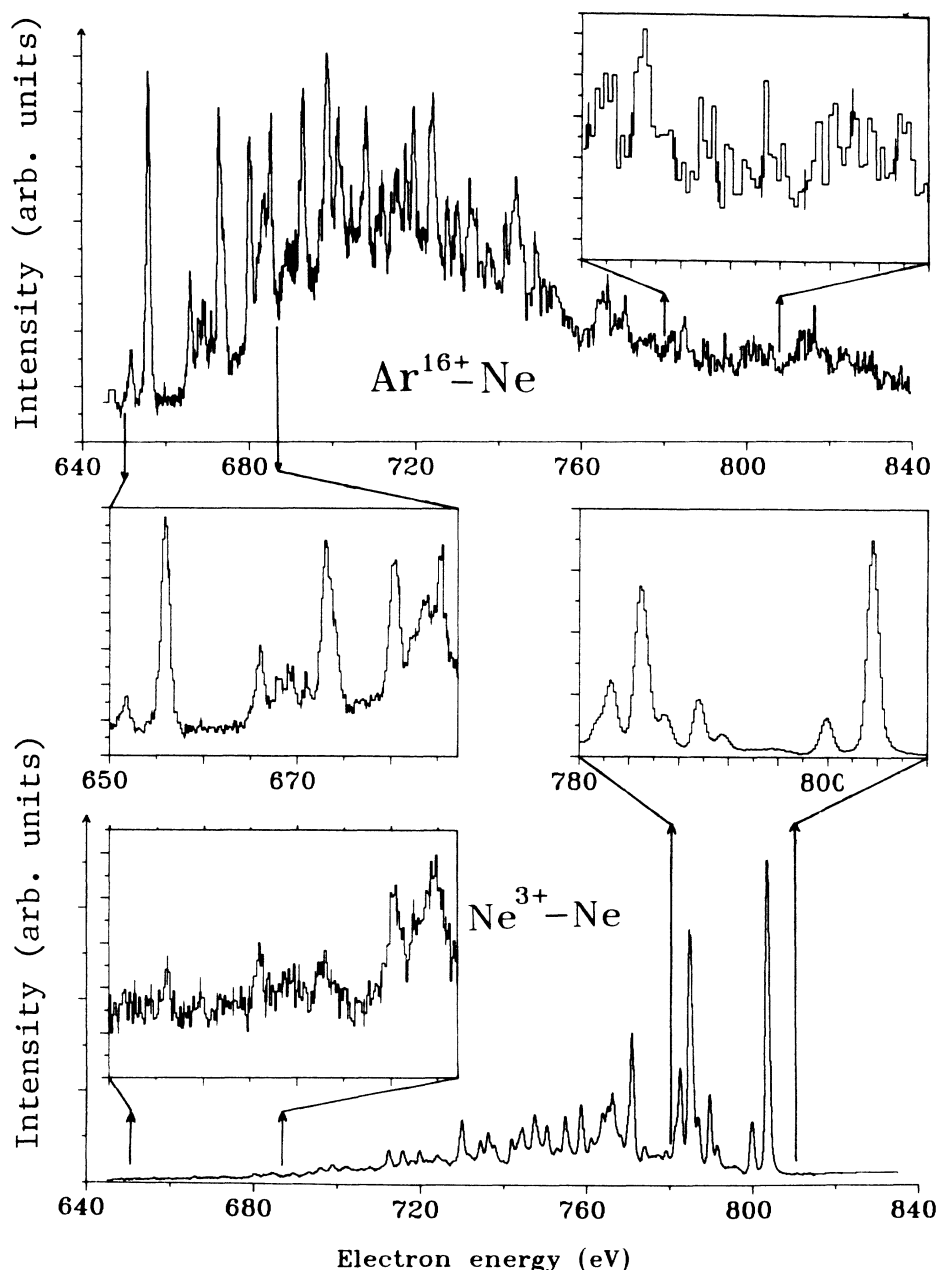

FIG. 2. Selected characteristic energy regions of the spectra measured in the Ar^{16+}-Ne and Ne^{3+}-Ne collisions at 5.5 MeV/u.

of transitions from the one L vacancy as well as the two and three L electron configurations. As can be seen in Fig. 2, these transitions produce prominent peaks in one spectrum while at the same time cause no detectable intensity in the other one. Supposing the (approximately) same intensity for the transitions from the same vacancy configuration (i.e., fixing the relative intensities $P_{m,k}$), we evaluate the one step more complicated spectra and check whether the previous tentative identification was correct or not. In these spectra new line energies and relative intensities can be determined. Bringing back this information to the previously evaluated, more simple spectrum, we can refine the intensity and energy values obtained this way until this iteration does not change the data any more. Continuing the procedure this way one can evaluate further target charge states, bearing in mind that it is not probable that all the transitions present in the spectrum will be identified. Finally using a consistent set of energy values we evaluated once more all the spectra, leaving free both parameters of the peaks, while the general parameters (B_0, B_1, σ) were kept constant. At the identification of the individual spectrum components we use not only their relative intensities in the given spectrum and their relative and absolute energy position, but the tendencies of their absolute and relative intensities found in the function of the projectile charge.

IV. IDENTIFICATION OF THE TRANSITIONS

The Ne KLL diagram lines are well known, measured with high precision,[28,35] so it is easy to identify them according to their energies. Most of the transitions originating from the one K one L hole initial states have been precisely measured by Krause, Carlson, and Moddeman[35] with electron and x-ray excitation.

The situation is quite different in the low-energy region. Here the peak around 656.5 eV serves as a good reference. The structure of the spectrum is simple in this region: there are only two prominent peaks to be found here, the one located at 656.6 eV and another one at 652.5 eV having significantly less intensity. Unfortunately, different theoretical calculations result in different energy values for these transitions and even their energetic order is changing according to the different theoretical methods.[36-38] Both transitions should be transitions from Li-like initial states since the smallest theoretical transition energy obtained for transitions from Be-like initial states gives 662.4 according to the calculation of Matthews, Johnson, and Moore[36] and according to the experimental evidence given by the measurement of Itoh et al.[15]

The energy values and relative intensities of transitions originating from the Li-, Be-, and B-like states[10,11] have been determined by target Auger spectroscopy only in a few cases, where the zero-degree Auger spectroscopical[15] and beam-foil[38] measurements of neon projectiles of different charge state are of great help in identifying the transitions. For the C- and N-like states, however, even less experimental data are available, since this is the most complex spectral region in the K Auger spectra. In this region we had to proceed by using theoretical predictions for the assignments.

As a first argument for the identification of the lines we used the ratio of their relative intensities and its dependence on the projectile charge to identify the target charge state they belong to. Using this for the first selection, the next argument was their succession and the respective calculated distances, as well as also their energy position. Furthermore, the experimental energy differences between given initial or final states evaluated from different transition pairs should agree within the limits of the experimental error. The differences obtained from optical measurements[39] were also used in this procedure. The next argument was that the magnitude of the population estimated for a given initial state from two different transitions should agree approximately. Finally, the measured angular distribution of Auger lines was used as additional information. The complete evaluation procedure on these data is under way, and the detailed results are to be published in a separate paper. However, we could use some of our earlier results[20,21,40,41] on angular distribution in the identification of the O-like lines. Furthermore, some new results on the angular distribution of all the measured Auger lines of the Ne^{3+} spectrum were used in the above analysis. For higher degrees of ionization only the high value of the measured anisotropy parameters was used as an exclusion condition for identifying a line as a transition originating from ^1S or ^2S initial states. In this way most of the electron lines could be assigned to a transition, eventually, however, more transitions could be assigned to the same line because of line blending, especially in the central energy region (where most of the transitions from N-, C-, and B-like configurations are located).

V. RESULTS

A. Spectroscopical data

The measured Ne KLL Auger line energies and intensities are given in Tables I–VII. In the individual tables a series of the corresponding theoretical values is also included which was calculated on the basis of one or the other approximation (see details later). The identification of the lines in the evaluation procedure was carried out as was described in Sec. IV. Considering that the measured spectra in the present study are the result of the superposition of many different transitions (except the H$^+$-Ne collision), those transitions are given in square brackets in the tables which coincide in energy with the identified transition concerned.

The experimental energy values in the tables are obtained by averaging the corresponding individual data measured at the impact of the different projectiles. The average deviation is indicated in parentheses after the energy values. The uncertainty in the energy calibration of the spectrometer is ±0.1 eV. The given relative intensities are normalized for the total intensity of the identified Auger transitions included in an individual table. In the second part of the individual tables the unidentified lines are listed which belong with high probability to the same initial L-shell vacancy state as the identified lines on the basis of the intensity ratio of the spectra taken at different projectiles, but a more specified identification could not

TABLE I. F-like diagram lines. (Initial state $1s^1 2s^2 2p^6\,^2S$).

Final state	Transition energy		Branching ratios Projectiles				
	$E_{\text{expt.}}$	E_{theor} [a]	Ne^{10+}	Ar^{6+}	Ne^{3+}	H^{+}	Theor. [a]
206 ^1S	748.41(2)	748.15	7.15(21)	5.0(2)	6.5(3)	5.92(30)	6.1
215 ^1P	771.86(2)	771.71	19.75(64)	14.9(5)	16.2(5)	17.25(31)	17.0
215 ^3P	782.24(3)	782.45	11.60(25)	10.2(3)	7.5(2)	6.27(28)	6.1
224 ^1S	800.73(4)	801.27	10.05(55)	11.1(4)	9.6(3)	9.69(12)	9.6
224 ^1D	804.50[b]	804.51	51.55(30)	58.8(25)	60.3(27)	60.88(76)	61.3
Total measured intensity			1571(70)	2191(48)	14 219(335)	117.24(66)	

[a]Kelly (Ref. 42).

[b]The energy scale was calibrated using this transition (Ref. 28).

be achieved. The given energy and intensity values here are determined as above. The total measured intensities of the groups of both the identified and not identified transitions are given in separate rows following the data blocks concerned. These quantities are normalized to 10^{12} incident particles.

In Table I there is a good agreement between the measured energies and branching ratios as well as the corresponding values calculated by Kelly,[42] who took into account the electron correlation, the relativistic and radiation corrections, the final-state configuration interaction. The maximum deviation between the experimental and theoretical energy values is 0.57 eV, while the average deviation is 0.23 eV. The branching ratios determined experimentally in the case of the different projectiles agree with the corresponding theoretical values within 20%. An exception is here the ^2S-^3P transition at Ar^{6+} and Ne^{10+} impact where the theoretical value is higher by a factor of 2. This deviation is probably caused by the admixture of a transition from a state of higher ionization.

In Tables II–IV the values concerned are given for the

Ne KLL Auger transitions originating from O-, N-, and C-like initial states. At the identification of the lines arising from initial states with one or two vacancies (O- or N-like states), the data of Krause, Carlson, and Moddeman[35] and those of the optical tables of Moore[39] were used. The theoretical energy values in Tables II–IV are the results of a single-configuration Dirac-Fock calculation,[37] which are in good agreement with the values of Matthews, Johnson, and Moore,[36] calculated in LS coupling and so it seemed to be unnecessary to include both series of values. The average deviation between the experimental and theoretical energy is 1.4 eV for O-like and 1.0 eV for N-like states. In Table IV where the theoretical values concerned were used at the identification, the above average deviation is 0.4 eV. To obtain the theoretical relative intensity values, the branching ratios of Bhalla[43] calculated in LS coupling and in addition the probabilities for multiple ionization from the geometrical model of Sulik et al.[24] as well as the statistic weight of the terms pertaining to a configuration were used. Thus

$$I_{ij}^{\text{theor}}(^{2S+1}L\,-\,^{2S'+1}L') = \frac{Q_{ij}B(^{2S+1}L\,-\,^{2S'+1}L')S(^{2S+1}L)}{\displaystyle\sum_{i,j}\sum_{S,S',L,L'} Q_{ij}B(^{2S+1}L\,-\,^{2S'+1}L')S(^{2S+1}L)} , \qquad (3)$$

where i, j is the number of electrons in the 2s and 2p shell, respectively, Q_{ij} the probability for production of the configuration concerned, $B(^{2S+1}L\,-\,^{2S'+1}L')$ is the branching ratio, and $S(^{2S+1}L)$ is the statistical weight. The summation in the denominator should be carried out for the observed transitions with k vacancies on the L shell, i.e., $i + j = k$. The relative intensity values calculated according to the above procedure can vary in dependence on the projectiles of different charge because Q_{ij} depends on the charge state of the impact ion. It can be shown, however, that the relative intensity values depend only on the ratio of the ionization probabilities for the 2s and 2p subshells, and this ratio does not depend strongly on the projectile charge (see the next sections). Therefore

only one column of theoretical intensity values belonging to Ne^{10+} impact is given in the tables. Comparing the experimental and theoretical intensity values in Tables II–IV, significant deviations can be observed. A possible reason for them is the deficiency both in the ionization theory and in the model for the decay of the states concerned.

The experimental and theoretical Auger energy values in Tables V–VII (B-, Be-, Li-like satellites) are in a very good agreement. Here the theoretical values are calculated in terms of multiconfiguration Dirac-Fock approximation.[44,38] The average deviations for B-, Be-, and Li-like states are, successively, 0.43, 0.48, and 0.38 eV. If the theoretical values for these states are taken according to

Maurer and Watson,[37] then the corresponding values for the deviation are 1.24, 1.16, and 1.43 eV, respectively. It shows the significant role of the electron correlation in these states. At the same time, it can be observed in Table V that there is not, in general, a significant deviation between the theoretical values for relative intensity calculated in different coupling schemes by Bhalla[43] as well as by Chen and Craseman.[44]

B. Multiple ionization and vacancy production

Studying the intensity of the Ne Auger KLL satellite transitions as a function of the projectile charge, information can be obtained on the multiple ionization process at small impact parameter. Namely, these satellites come into being when in addition to the vacancy in the K shell holes are also produced in the L shell. Thus the effective impact-parameter region for the whole process is determined by the K-shell ionization, therefore, it is much smaller than in the case of L-shell ionization in general.

The description of multiple ionization is a difficult task because the issue to be solved is a many-body problem. For the time being there are two ways for the solution of the problem: one of them is the coupled-channel quantum-mechanical approximation[45] and the other one is a statistical approach.[46] In the latter case it is supposed that the ejection of n electrons from the L shell in addition to those from the K shell is described by the binomial distribution, i.e.,

$$\sigma_{K,nL} = 4\pi \int_0^\infty p_K(b)[1-p_K(b)]\begin{bmatrix}8\\n\end{bmatrix}p_L^n(b)$$
$$\times[1-p_L(b)]^{8-n}b\,db\,,\qquad(4)$$

where $\sigma_{K,nL}$ is the cross section for K-shell ionization with simultaneous ejection of n electrons from the L shell, $p_K(b)$ and $p_L(b)$ are the ionization probabilities at impact parameter b, respectively. The total K ionization cross section is

$$\sigma_K = \sum_n \sigma_{K,nL}\,.\qquad(5)$$

TABLE II. O-like and N-like satellite lines. The transitions in square brackets are also possible energetically.

State		Transition energy		Relative intensities Projectiles				
Initial	Final	$E_{expt.}$	$E_{theor.}$ [a]	Ne^{10+}	Ar^{6+}	Ne^{3+}	H^+	Theor.[b]
$125\,^3P-205\,^2P$		730.95(2)	731.30	10.3(3)	9.6(3)	6.7(2)	5.24(17)	7.34
$125\,^3P-214\,^2P$		751.41(3)	751.00	6.4(2)	6.0(2)	5.4(2)	3.90(21)	6.70
$[124\,^2D-213\,^3D]$			(751.10)					
$125\,^3P-214\,^2D$		759.62(9)	760.20	11.1(3)	9.8(4)	8.9(3)	7.25(38)	8.34
$125\,^3P-214\,^4P$		768.32(8)	770.30	4.3(1)	4.1(1)	4.2(1)	2.35(32)	3.30
$125\,^3P-223\,^2P$		783.29(1)	784.10	8.8(3)	9.5(3)	10.2(3)	11.67(15)	10.76
$125\,^3P-223\,^2D$		785.86(2)	787.80	22.1(10)	24.5(10)	26.7(15)	21.05(186)	24.67
$125\,^1P-205\,^2P$		735.41(4)	735.40	9.3(3)	7.9(2)	4.0(1)	3.75(24)	2.62
$[114\,^1P-203\,^2P]$			(735.20)					
$[114\,^1S-203\,^2P]$			(735.40)					
$125\,^1P-214\,^2P$		755.67(3)	755.10	9.4(3)	8.1(2)	6.9(2)	8.02(66)	5.43
$[115\,^2P^- -204\,^3P]$			(755.10)					
$125\,^1P-214\,^2D$		763.71(4)	764.30	3.1(3)	2.7(1)	3.0(1)	2.03(45)	0.00
$125\,^1P-223\,^2P$		787.84(2)	788.20	3.3(1)	3.7(1)	5.4(2)	8.64(17)	3.90
$125\,^1P-223\,^2D$		790.46(1)	791.90	7.4(3)	8.3(3)	10.1(3)	13.76(16)	8.94
$116\,^3S-214\,^2D$		785.35(6)	788.20	3.6(1)	4.5(2)	6.1(2)	7.64(39)	13.47
$116\,^1S-214\,^2D$		792.36(1)	795.70	1.10(3)	1.34(4)	2.45(8)	4.32(45)	4.49
Identified total intensity				8295(81)	8709(103)	21 241(325)	17.55(117)	
Not identified O-like lines								
		771.57(3)		40.7(13)	42.0(12)	30.3(8)		
		779.84(4)		7.2(2)	6.3(2)	6.9(2)		
		780.17(3)		8.4(4)	7.7(2)	6.1(2)		
		783.68(3)		16.3(7)	15.1(4)	17.5(5)		
		786.55(6)		10.8(7)	11.4(4)	19.0(5)		
		791.69(1)		3.6(4)	4.1(1)	4.5(1)		
		792.69(7)		4.5(1)	4.6(1)	4.3(1)		
		793.92(6)		1.3(1)	1.2(1)	1.8(1)		
		796.65(5)		2.6(3)	2.3(1)	3.5(1)		
		797.51(2)		2.2(1)	2.0(1)	2.1(1)		
		800.16(4)		2.5(1)	3.3(1)	4.0(1)		
Not identified total intensity				1458(18)	1696(22)	4876(51)		

[a]Maurer and Watson (Ref. 37).
[b]Bhalla (Ref. 43).

TABLE III. N-like satellite lines. The transitions in square brackets are also possible energetically.

State Initial	State Final	Transition energy $E_{expt.}$	E_{theor} [a]	Relative intensities Projectiles Ne^{10+}	Ar^{6+}	Ne^{3+}	Theor. [b]
124 ^4P	204 ^3P	713.06(12)	714.90	4.51(13)	4.33(12)	3.90(9)	4.59
124 ^4P	213 ^3S	730.25(9)	730.70	2.15(5)	1.95(5)	2.58(7)	1.71
124 ^4P	213 ^3P	738.84(3)	740.90	6.54(19)	6.24(19)	4.64(18)	3.22
[124 ^2P	213 ^1D]		(738.40)				
[123 ^3P	212 ^4P]		(739.00)				
124 ^4P	213 ^3D	742.48(4)	744.80	3.23(11)	3.45(13)	2.16(5)	5.36
124 ^4P	213 ^5S	753.09(1)	757.40	2.73(9)	2.56(7)	1.44(3)	0.98
[125 ^3P	214 ^2S]		(754.70)				
124 ^4P	222 ^3P	764.50(3)	766.00	5.45(21)	5.79(21)	6.61(19)	11.82
124 ^2D	204 ^1D	717.14(4)	717.30	4.47(16)	3.95(11)	2.91(11)	3.24
124 ^2D	213 ^1D	739.76(3)	737.80	2.89(8)	2.59(8)	1.94(5)	3.86
[114 ^1P	203 ^2D]		(739.40)				
124 ^2D	222 ^1S	764.90(5)	762.30	4.60(37)	4.18(11)	4.91(13)	1.55
124 ^2D	222 ^1D	769.29(2)	768.30	4.43(9)	5.06(14)	6.08(16)	11.44
124 ^2P	204 ^3P	720.65(1)	721.80	6.79(40)	6.83(20)	4.35(12)	2.67
[114 ^3D	203 ^3P]		(720.50)				
124 ^2P	213 ^1P	734.42(5)	734.40	3.98(13)	3.84(11)	2.47(11)	0.35
124 ^2P	213 ^3S	737.21(1)	737.60	5.87(17)	5.57(15)	6.36(19)	3.00
124 ^2P	213 ^3D	749.95(3)	751.70	5.38(40)	5.89(15)	4.08(11)	0.21
[114 ^1D	212 ^2S]		(749.90)				
124 ^2P	222 ^3P	772.13(2)	772.90	3.15(15)	3.13(12)	2.41(6)	6.89
124 ^2S	213 ^1P	740.96(3)	739.80	2.51(9)	2.28(6)	1.76(4)	1.18
115 ^4P	204 ^3P	737.92(4)	738.30	3.35(8)	3.25(8)	3.07(8)	1.35
115 ^4P	213 ^3P	762.97(8)	764.30	3.49(17)	3.67(9)	3.84(9)	5.83
115 ^4P	213 ^3D	767.03(6)	768.20	8.00(52)	8.55(24)	12.26(33)	13.46
115 $^2P^+$	204 ^3P	747.84(4)	747.50	4.11(11)	4.01(11)	4.33(14)	2.43
[114 ^3S	212 ^2S]		(747.70)				
[124 ^2P	213 ^3P]		(747.80)				
[105 ^3P	203 ^2P]		(747.60)				
115 $^2P^+$	213 ^1P	761.93(2)	760.10	5.96(22)	5.89(16)	5.88(17)	1.70
[114 ^1S	212 ^2D]		(762.50)				
115 $^2P^+$	213 ^1D	765.75(5)	764.10	5.23(14)	4.68(13)	7.52(19)	3.92
115 $^2P^-$	213 ^1D	773.22(4)	771.70	1.02(9)	1.02(2)	1.78(4)	0.16
[106 ^2S	204 ^1D]		(772.80)				
115 $^2P^-$	213 ^3P	781.06(3)	781.10	1.10(3)	1.09(3)	2.12(5)	2.75
115 $^2P^-$	213 ^3D	784.44(9)	785.00	0.20(5)	0.21(2)	0.60(1)	6.30
Identified total intensity				13 341(532)	13 010(80)	14 859(95)	

Not identified N-like lines

$E_{expt.}$	Ne^{10+}	Ar^{6+}	Ne^{3+}
713.53(1)	7.91(32)	7.85(22)	0.91(4)
753.73(4)	9.90(57)	9.56(28)	10.68(27)
757.52(3)	11.49(59)	10.54(28)	8.86(22)
758.59(4)	12.23(50)	12.10(33)	9.36(24)
760.70(2)	7.81(23)	8.01(21)	8.84(24)
766.14(11)	17.26(106)	17.63(50)	13.65(35)
775.06(3)	7.99(41)	7.39(19)	9.31(23)
776.11(3)	5.01(17)	4.90(13)	6.96(18)
777.07(2)	5.01(19)	5.52(14)	7.77(20)
778.07(3)	6.44(34)	6.01(16)	8.43(22)
778.90(5)	3.27(37)	3.38(9)	5.16(13)
787.55(4)	3.18(13)	4.07(11)	5.69(14)
795.32(5)	0.90(3)	1.05(4)	1.56(4)
795.94(3)	1.14(3)	1.36(4)	2.32(6)
798.07(4)	0.50(4)	0.63(4)	0.49(3)
Not identified total intensity	4221(177)	3891(32)	5106(37)

[a] Maurer and Watson (Ref. 37).
[b] Bhalla (Ref. 43).

TABLE IV. C-like satellite lines. The transitions in square brackets are also possible energetically.

| State | | Transition energy | | Relative intensities Projectiles | | | |
Initial	Final	$E_{\text{expt.}}$	E_{theor} [a]	Ne^{10+}	Ar^{6+}	Ne^{3+}	Theor.[b]
	$123\,^5S-203\,^4S$	697.93(7)	698.00	2.23(9)	2.48(7)	1.36(3)	4.05
	$123\,^5S-212\,^2P$	705.51(3)	704.90	2.47(6)	2.26(6)	0.97(3)	1.84
	$[113\,^6S-211\,^3P]$		(706.20)				
	$123\,^3D-203\,^2D$	700.78(18)	700.70	2.82(8)	2.74(9)	1.80(5)	4.11
	$123\,^3D-212\,^2P$	714.05(7)	713.90	2.71(7)	2.67(7)	2.60(7)	2.03
	$123\,^3D-212\,^2D$	722.40(3)	723.60	3.28(15)	3.26(9)	2.79(8)	4.45
	$123\,^3D-212\,^4P$	732.43(3)	734.70	1.42(6)	1.46(4)	3.63(9)	0.95
	$[114\,^3P^--203\,^2P]$		(731.50)				
	$123\,^3D-221\,^2P$	744.91(4)	744.90	5.75(45)	6.71(18)	6.04(17)	11.43
	$123\,^1D-203\,^2D$	706.47(6)	705.90	2.25(11)	2.38(6)	1.48(4)	1.61
	$[123\,^1P-203\,^2P]$		(706.00)				
	$[113\,^2D^+-202\,^1D]$		(706.30)				
	$123\,^1D-221\,^2P$	750.74(4)	750.10	3.06(53)	2.97(8)	3.19(10)	3.62
	$123\,^3S-203\,^4S$	708.04(6)	708.40	2.05(6)	2.18(6)	1.39(4)	2.38
	$123\,^3S-212\,^2P$	715.20(6)	715.30	3.03(7)	3.05(9)	2.26(7)	1.16
	$123\,^3P-212\,^2p$	718.47(2)	718.20	3.38(9)	3.42(12)	2.53(7)	1.38
	$[113\,^2P^--202\,^1D]$		(718.40)				
	$123\,^3P-212\,^2D$	727.03(3)	727.90	3.19(8)	3.14(8)	2.92(8)	1.69
	$[114\,^3S-203\,^2P]$		(726.90)				
	$[113\,^4P-211\,^3P]$		(727.40)				
	$123\,^3P-221\,^2P$	748.93(3)	749.20	4.55(17)	4.92(14)	6.78(20)	4.64
	$123\,^1P-212\,^2S$	726.04(3)	726.80	3.69(29)	3.36(9)	2.89(7)	1.21
	$[123\,^5S-212\,^4P]$		(725.70)				
	$114\,^5P-203\,^4S$	717.78(2)	717.40	0.70(4)	0.70(2)	0.67(2)	1.00
	$114\,^5P-212\,^4P$	745.66(4)	745.10	7.58(74)	7.02(21)	8.34(22)	14.32
	$114\,^3P^+-203\,^2P$	719.35(3)	719.10	3.78(18)	3.65(12)	2.86(7)	1.38
	$[123\,^1D-212\,^2P]$		(719.10)				
	$[113\,^2D^+-211\,^1P]$		(719.20)				

Since $p_L(b)$ is regarded constant $[p_L(b)=p_L(0)$ in the impact-parameter region determined by K-shell ionization], the expression characterizing the L-shell ionization can be taken out from the integration. Let us introduce the relative cross section Q_n of producing n holes in the L shell, accompanied with one K hole as

$$Q_n = \frac{\sigma_{K,nL}}{\sigma_K} = \binom{8}{n} p_L^n(0)[1-p_L(0)]^{8-n},$$

$$\sum_{n=0}^{8} Q_n = 1. \tag{6}$$

Thus the solution of the many-body problem is reduced for the determination of $p_L(0)$.

In the Auger and x-ray spectroscopical studies of moderate energy resolution (cf., e.g., Refs. 12 and 47), the $p_L(0)$ values are determined by relation (6) in the collisions with multiple ionization. In the determination of $p_L(0)$ based on the detection of the x rays in the case of targets of low atomic number (as also Ne), the fluorescence yield depending on the degree of ionization can be a source of a significant error. At the detection of Auger spectra, however, the phenomenon concerned influences

the $p_L(0)$ value much less.

Equation (6) supposes tacitly that the ionization probabilities for the $2s$ and $2p$ subshells are equal. If the instrumental energy resolution is high enough, then the validity of this supposition can be checked. In one of our former works [19] it was shown based on the evaluation of the Ne KLL diagram and one L hole satellite Auger lines that the p_{2s} and p_{2p} ionization probabilities are different. This means that beside equation (6) the following double binomial distribution should be used in the description of the multiple ionization concerned:

$$Q_{ij} = \binom{2}{i} p_{2s}^i(0)[1-p_{2s}(0)]^{2-i} \binom{6}{j} p_{2p}^j(0)[1-p_{2p}(0)]^{6-j},$$

$$\tag{7}$$

where i is the number of holes produced in the $2s$ subshell (accompanying a hole in the K shell) and j is that in the $2p$ subshell, and $p_{2s}(0)$ and $p_{2p}(0)$ are the ionization probability for the same subshells, respectively.

The theoretical description and the evaluation of the experiment are even more complicated if, in addition to the ionization processes, other channels which produce L holes are also present (e.g., excitation to higher bound

TABLE IV. (*Continued*).

| State | | Transition energy | | Relative intensities Projectiles | | | |
Initial	Final	$E_{\text{expt.}}$	$E_{\text{theor.}}$[a]	Ne^{10+}	Ar^{6+}	Ne^{3+}	Theor.[b]
$114\,^3P^+$	$-203\,^2D$	723.31(3)	723.30	3.78(17)	3.25(8)	2.74(8)	2.30
$114\,^3P^+$	$-212\,^2P$	736.21(6)	736.50	2.38(32)	2.21(6)	2.46(7)	4.36
$114\,^3P^+$	$-212\,^4P$	754.67(7)	757.30	3.67(10)	3.47(10)	3.84(10)	0.05
$[123\,^1P$	$-221\,^2P]$		(754.40)				
$114\,^3D$	$-203\,^2D$	724.36(2)	724.70	3.79(11)	4.46(12)	2.80(7)	0.32
$114\,^3D$	$-212\,^2S$	740.38(3)	741.30	1.09(03)	1.07(3)	0.86(2)	1.70
$114\,^3D$	$-212\,^2D$	746.76(2)	747.60	5.17(18)	5.27(15)	5.26(15)	12.55
$114\,^1D$	$-203\,^2P$	728.82(3)	729.10	3.17(16)	3.14(8)	2.80(7)	0.56
$114\,^1D$	$-203\,^2D$	733.51(12)	733.30	2.64(27)	2.67(7)	3.42(10)	1.68
$114\,^1D$	$-212\,^2D$	756.56(5)	756.20	2.53(16)	2.59(7)	4.87(15)	2.58
$[114\,^1P$	$-212\,^2S]$		(756.00)				
$114\,^3P^-$	$-203\,^4S$	742.99(2)	742.00	6.81(26)	5.76(17)	6.62(17)	1.03
$[115\,^2P^+$	$-204\,^1D]$		(743.60)				
$114\,^3P^-$	$-212\,^4P$	770.64(6)	769.70	4.29(15)	4.91(18)	7.26(18)	7.16
$105\,^3P$	$-203\,^2D$	752.25(2)	751.80	2.82(12)	2.84(7)	2.54(6)	3.02
$[105\,^1P$	$-203\,^2P]$		(752.60)				
Identified total intensity				15 380(205)	14 535(80)	11 744(65)	
Not identified C-like lines							
		695.77(7)		7.22(23)	5.66(15)	4.41(11)	
		696.86(4)		8.93(36)	8.65(23)	9.80(25)	
		702.77(19)		10.35(88)	10.97(31)	8.46(22)	
		709.97(3)		7.43(19)	7.37(20)	4.18(11)	
		710.98(8)		7.25(22)	8.26(22)	7.08(18)	
		712.01(3)		10.61(27)	9.77(26)	10.61(28)	
		716.31(8)		15.44(47)	16.64(57)	19.09(58)	
		725.20(5)		16.81(85)	16.34(44)	16.24(43)	
		744.10(3)		15.98(64)	16.33(44)	20.12(52)	
Not identified total intensity				4377(60)	4161(40)	2618(25)	

[a]Maurer and Watson (Ref. 37).
[b]Bhalla (Ref. 43).

states of the target). In such a case the $p_{2s}(0)$ and $p_{2p}(0)$ in Eq. (7) denote vacancy production probabilities, respectively, instead of ionization probabilities. That is, the vacancy production probability $p^{(v)}$ is

$$p^{(v)} = p^{(i)} + p^{(e)} , \qquad (8)$$

where $p^{(i)}$ and $p^{(e)}$ are the probabilities of the ionization and other vacancy production processes, respectively, for a given subshell. If Eq. (8) will be substituted in Eq. (7), then the relative intensity of the satellite lines of nm hole originating from pure Coulomb ionization $Q_{nm}^{(i)}$ is as follows:

$$Q_{nm}^{(i)} = \begin{bmatrix} 2 \\ n \end{bmatrix} p_{2s}^{(i)\,n}(0)[1 - p_{2s}^{(v)}(0)]^{2-n} \begin{bmatrix} 6 \\ m \end{bmatrix}$$
$$\times p_{2p}^{(i)\,m}(0)[1 - p_{2p}^{(v)}(0)]^{6-m} , \qquad (9)$$

while

$$\sum_{n,m} Q_{nm} = [1 - p_{2s}^{(e)}(0)]^2 [1 - p_{2p}^{(e)}(0)]^6 . \qquad (10)$$

The ratio of Eq. (9) to Eq. (10) (after simple substitution)

will give a binomial distribution of two parameters which is of the same shape as Eq. (7) if the following substitutions are applied:

$$p_{2s} = p_{2s}^{(i')} = \frac{p_{2s}^{(i)}}{1 - p_{2s}^{(e)}} , \quad p_{2p} = p_{2p}^{(i')} = \frac{p_{2p}^{(i)}}{1 - p_{2p}^{(e)}} . \qquad (11)$$

The parameters of the double binomial distribution according to Eq. (7) were determined by using the data included in Tables I–VII. In this procedure the branching ratios calculated by Bhalla,[43] the statistical weight for the nonobserved states, and the fluorescence yield by Chen and Craseman[48] were used. In the distribution as well as during the fitting procedure only the reliably identified transitions were taken into consideration in which there was no admixture from other transition(s) (cf. Tables I–VII, transitions without alternative identification in square brackets).

Since for the part of the present collision systems the SCA or BEA approximations result in $p_L(0)$ values higher than unity, in Eq. (6) negative values for Q_n can be obtained in the case of impact ions with high charge

TABLE V. B-like satellite lines. The transitions in square brackets are also possible energetically.

| State | | Transition energy | | | Relative intensities | | | |
Initial	Final	E_{expt}	$E_{theor.}$ [a]	Ne^{10+}	Projectiles Ar^{6+}	Ne^{3+}	Theor.$_1$ [b]	Theor.$_2$ [a]
$122\,^4P$–$202\,^3P$		681.87(5)	682.80	3.50(11)	4.02(11)	2.37(9)	8.31	10.21
$122\,^4P$–$211\,^3p$		704.60(12)	705.10	6.98(31)	6.85(18)	10.40(27)	12.56	12.48
$122\,^2D$–$202\,^1D$		684.94(6)	685.62	6.40(57)	6.87(18)	5.35(14)	4.78	6.16
$122\,^2D$–$211\,^1P$		698.98(13)	698.08	9.47(39)	10.35(28)	5.73(16)	4.02	3.78
$122\,^2P$–$202\,^3P$ $[122\,^2D$–$202\,^3P]$		690.06(2)	691.20 (690.20)	8.13(42)	9.41(25)	7.07(18)	7.63	8.43
$113\,^6S$–$211\,^1P$		691.03(5)	691.43	5.82(23)	5.61(15)	4.19(11)	0.00	0.00
$113\,^4S^+$–$202\,^3P$ $[113\,^4D$–$202\,^3P]$		699.87(18)	699.45 (700.10)	19.19(83)	18.61(81)	19.55(51)	5.15	5.58
$113\,^4D$–$211\,^3P$		721.50(2)	722.40	11.54(57)	11.33(35)	15.69(40)	23.73	25.71
$113\,^2D^-$–$211\,^3P$		741.65(5)	740.65	5.76(34)	5.05(16)	6.78(18)	8.34	0.31
$104\,^4P$–$202\,^3P$		727.91(7)	728.40	8.66(39)	7.79(23)	9.70(31)	11.43	12.22
$104\,^2D$–$202\,^1D$		731.77(4)	731.18	11.43(49)	10.66(38)	11.13(31)	8.37	8.89
$104\,^2P$–$202\,^3P$		736.80(3)	736.80	3.24(11)	3.46(9)	2.05(12)	5.70	6.14
Identified total intensity				3782(96)	3541(38)	1553(13)		
Not identified B-like lines								
		679.11(2)		4.76(30)	3.99(11)	0.89(30)		
		680.34(14)		6.49(33)	7.02(20)	3.92(32)		
		693.15(5)		15.30(40)	16.53(46)	14.91(41)		
		707.20(5)		18.17(82)	16.56(47)	20.27(57)		
		729.61(6)		25.61(103)	25.75(72)	22.57(62)		
		767.51(2)		29.68(154)	30.15(95)	37.44(103)		
Not identified total intensity				1496(48)	1463(18)	457(6)		

[a]Chen and Craseman (Ref. 44).
[b]Bhalla (Ref. 43).

(namely, the ionization probability should be multiplied by the square of the ion charge), which is quite unreasonable. This contradiction is eliminated by the semiclassical geometrical model of Sulik et al.[24] It was shown that the results of the latter model are in a good agreement with those of Becker, Ford, and Reading[45] in the impact energy region above 1 MeV/u. In the present paper the geometrical model is used for the interpretation of the experimental results. This approximation can be applied in the case of bare projectiles without any further consideration. If the projectile, however, has got accompanying electron(s), then a proper procedure is needed to determine the effective ion charge (Z_{eff}) which is characteristic of the collision concerned. To obtain Z_{eff} for Ne^{3+}, Ar^{6+}, and Ar^{16+}, the procedure described in Sec. 2.4 of Hock et al.'s work[49] was used.

The geometrical model is supposed to give account only of the ionization probabilities $p_{nl}^{(i)}$. The present form of this model cannot determine theoretical excitation probabilities $p_{nl}^{(e)}$ and there are no other simple theories for multiple excitation in this projectile charge region. Therefore we can give only a partial comparison of experiment and theory. Table VIII shows the experimentally

determined probability parameters of the distributions p_{2s} and p_{2p} and the ionization probabilities calculated by using the geometrical model $p_{2s}^{(i)}$ and $p_{2p}^{(i)}$. Conceptually they are different quantities [see Eq. (11)] but, as was pointed out in an earlier study,[19] their values do not differ from each other more than a few percent in the cases of the present collision systems.

There is physically relevant information as to how good the double binomial distribution of Eq. (9) is for the description of the experimentally determined distribution in detail. The present study is the first one in which two-dimensional vacancy configuration distributions were determined experimentally for all the configurations attainable by Auger transitions in the case of Ne^{3+}, Ne^{10+}, and Ar^{6+} projectiles. This may give a unique possibility to analyze the multiple vacancy production mechanism, keeping in mind that the experimental distributions certainly involve some of the systematic errors originating from the model errors of the fitting procedure, from erroneous line identifications, from inaccurate theoretical branching ratios, etc. Figure 3 displays the comparison of these distributions with both the fitted double binomial and the theoretical ones, calculated according to the

TABLE VI. Be-like satellite lines.

State Initial	Final	Transition energy $E_{expt.}$	$E_{theor.}$[a]	Branching ratios Projectiles Ar^{16+}	Ne^{10+}	Ar^{6+}	Ne^{3+}	Theor.[b]
121 ^3P–201	^2P	666.88(1)	667.83	6.06(14)	5.65(28)	6.37(16)	4.61(16)	10.72
121 ^3P–210	^2S	683.05(10)	683.97	5.99(14)	6.78(28)	6.30(16)	5.60(17)	7.98
121 ^1P–201	^2P	673.62(7)	674.17	8.40(20)	6.20(33)	8.10(21)	3.29(13)	6.22
112 ^5P–201	^2P	669.86(5)	670.13	4.29(10)	3.12(8)	3.10(8)	2.33(16)	0.00
112 ^5P–210	^2S	685.75(6)	686.31	10.03(26)	8.96(23)	8.59(22)	10.36(27)	0.00
112 $^3P^+$–201	^2P	684.05(7)	684.57	7.13(17)	6.83(16)	7.60(20)	5.70(15)	14.42
112 ^3D–201	^2P	686.64(5)	685.28	5.24(14)	6.10(30)	5.91(16)	3.60(15)	2.73
112 ^3D–210	^2S	702.00(13)	701.42	11.86(37)	13.94(103)	14.66(43)	19.66(51)	21.31
112 ^3S–201	^2P	692.09(5)	692.34	6.26(15)	5.27(23)	4.90(13)	1.89(16)	3.64
112 ^1D–201	^2P	694.94(4)	694.71	3.61(10)	5.02(40)	4.52(12)	2.00(15)	4.04
103 ^5S–201	^2P	693.95(6)	693.81	12.22(29)	12.02(69)	12.75(33)	13.43(34)	5.79
103 ^3D–201	^2P	703.65(18)	703.90	10.17(25)	14.88(49)	12.21(32)	19.48(56)	17.36
103 ^1D–201	^2P	709.34(4)	710.00	8.74(21)	5.26(15)	4.99(13)	8.05(21)	5.79
Identified total intensity				16 691(120)	2978(46)	2995(24)	963(9)	
Not identified Be-like lines								
		671.66(2)		22.13(57)	16.02(96)	16.82(47)	2.44(169)	
		676.22(2)		13.33(34)	12.33(53)	11.87(46)	0.16(179)	
		687.63(4)		26.54(71)	30.70(79)	30.15(85)	27.45(176)	
		688.88(3)		38.00(103)	40.96(93)	41.16(116)	69.94(289)	
Not identified total intensity				2469(31)	415(25)	386(5)	85(3)	

[a]Chen and Craseman (Ref. 44).
[b]Bhalla (Ref. 43).

geometrical model, for projectiles giving full distributions of Auger-detectable vacancy configurations (Ne^{3+}, Ar^{6+}, and Ne^{10+}). The numerical values and errors of the experimental vacancy configuration distributions are given in Table IX. It can be seen that the agreement between the measured and fitted distributions is not within the estimated uncertainty but one cannot find any significant differences between them. This result suggests that the contribution of the systematic errors is dominant and—at least regarding the vacancy configuration distributions—the independent-particle model cannot be rejected in this projectile velocity region even for high projectile charges.

TABLE VII. Li-like satellite lines.

State Initial	Final	Transition energy $E_{expt.}$	E_{theor}[a]	$E_{theor.}$[b]	Branching ratios Projectiles Ar^{16+}	Ne^{10+}	Ar^{6+}	Ne^{3+}	Theor.[c]
120 ^2S–200	^1S	652.47(2)	656.40	652.7	5.40(14)	5.82(21)	5.25(21)	3.00(88)	7.40
111 ^4P–200	^1S	656.59(2)	656.20	656.3	36.78(98)	27.53(66)	31.64(90)	13.71(105)	28.94
111 $^2P^+$–200	^1S	668.75(4)	668.70	668.9	8.47(23)	8.90(49)	10.13(30)	4.18(102)	14.47
111 $^2P^-$–200	^1S	672.70(4)	675.80	673.1	3.64(10)	3.55(52)	4.00(24)	1.78(88)	14.47
102 ^4P–200	^1S	674.05(8)	673.90	673.5	16.68(45)	3.63(35)	4.67(28)	10.45(88)	18.93
102 ^2D–200	^1S	681.16(3)	682.30	681.8	29.03(122)	50.45(126)	44.17(126)	66.68(247)	15.78
Identified total intensity					7239(107)	590(37)	688(10)	146(4)	
Not identified Li-like lines									
		660.35(2)			4.82(13)				
		662.23(1)			4.82(13)				
		665.66(7)			9.73(26)	6.79(167)	8.74(75)		
		670.71(2)			8.03(21)	5.00(130)	4.06(83)		
		674.65(10)			45.41(120)	57.09(202)	60.85(204)		
		677.58(7)			18.11(47)	23.77(229)	23.05(114)		
		678.54(9)			9.07(24)	7.35(75)	3.29(86)		
Not identified total intensity					1751(21)	149(16)	153(3)		

[a]Maurer and Watson (Ref. 37).
[b]Schumann, Groeneveld, and Nolte (Ref. 38).
[c]Bhalla (Ref. 43).

KÁDÁR, RICZ, VÉGH, SULIK, VARGA, AND BERÉNYI

TABLE VIII. Experimental and theoretical (Ref. 24) ionization probabilities.

Projectile	Experiment[a]		Theory (Ref. 24)	
	p_{2s}	p_{2p}	$p_{2s}^{(i)}$	$p_{2p}^{(i)}$
H^+	0.010(1)	0.023(1)	0.011	0.005
Ne^{3+}	0.162(4)	0.226(5)	0.151	0.157
Ne^{10+}	0.227(4)	0.377(3)	0.300	0.382
Ar^{6+}	0.237(4)	0.364(3)	0.216	0.273
Ar^{16+}	0.400(4)	0.453(3)	0.491	0.589

[a]Results of a two-parameter least-squares fitting procedure using Eq. (9) over the experimental distributions given in Table IX. The numbers in parentheses are pure statistical errors (1σ level).

The data of Table VIII suggest that the geometrical model of ionization is quite good for strongly ionizing collisions (for heavy-ion impact the maximum deviance in ionization probabilities is 40%) but it somehow breaks down just for the proton bombardment case where the interaction in the collision is the weakest one. For this latter case the model gives a good p_{2s} probability but it roughly underestimates the p_{2p} value. The most probable explanation of this discrepancy is that the geometrical model does not take into account the shake-off and shake-up processes which may become dominant for the outermost subshell for proton impact. It is necessary to mention here that the corresponding ionization probabilities calculated by using the most common BEA method[46] are even lower for the proton case, and much higher for Ar^{16+} impact, than the results of the geometrical model. Looking at Fig. 3 one may have the impression that, for the dominating members of the vacancy distributions, the prediction of the geometrical model gives not much worse agreement than the double binomial distribution fitted to the experimental data.

There is a physically interesting question too, whether the change of the effective binding energy of L-shell electrons, which should be an increasing function of the degree of ionization, does play any role in the determination of the shape of the experimental distribution. Having the measured vacancy-configuration distributions concerned we may try to investigate this often occurring but experimentally not answered question for ionization probabilities. In order to analyze our data from this point of view we calculated the parameters p_{2s} and p_{2p} for every possible pair of neighboring members of the experimental distributions on the basis of Eq. (9). We could not find any significant tendency in the values of either p_{2s} or p_{2p} as a function of the degree of multiple ionization. An illustration of the above results is given in Fig. 4 where the dependences of p_{2p} values on the number of the L vacancies are shown for different projectiles.

This result is quite surprising because semiclassical Monte Carlo calculations for multiple-ionization cross sections and their comparison to the experiments[50] show that a strong dependence of the one-electron ionization cross section on the degree of ionization was necessary to take into account, in the calculations, the reproducing of the experimental data. A possible explanation of this contradiction may come from the fact that in Ref. 50 multiple ionization is not connected to the small-impact-parameter region, while in the present study we really measured the probabilities at nearly zero impact parameter.

VI. CONCLUSIONS

A series of complex, high-resolution K Auger spectra of neon target was measured, excited by different fast projectiles with the same impact velocity. The characteristic property of the high-resolution Auger spectrosco-

TABLE IX. Experimental vacancy-configuration distribution (%).

Conf.[a]	H^+	Ne^{3+}	Ne^{10+}	Ar^{6+}	Ar^{16+}
100	85.5(5)	20.4(5)	3.0(2)	4.3(1)	
110	1.8(2)	3.1(1)	0.89(3)	1.17(5)	
120		0.42(2)	0.29(3)	0.28(1)	
101	11.9(12)	28.1(8)	13.5(3)	14.9(4)	
111		9.1(2)	7.9(4)	7.6(2)	
121		1.00(3)	1.44(9)	1.38(4)	
102		13.7(2)	18.8(8)	17.9(2)	
112		8.7(1)	13.7(4)	13.1(2)	
122		0.69(2)	2.2(1)	1.92(6)	
103		8.4(2)	14.9(4)	14.4(2)	
113		2.66(6)	7.7(4)	7.0(3)	
123		0.79(2)	2.4(1)	2.08(5)	4.7(1)
104		1.42(3)	5.9(3)	6.2(2)	
114		0.96(3)	4.5(2)	4.6(1)	8.3(2)
124		0.23(2)	0.87(7)	0.93(3)	3.35(9)
105		0.16(1)	0.97(4)	1.18(3)	2.36(5)
115		0.05(1)	0.59(4)	0.79(2)	3.23(9)
106		0.006(2)	0.06(1)	0.07(1)	0.28(1)

[a]Vacancy configurations, i.e., the corresponding electron configuration of 105 is $1s^1 2s^2 2p^1$. The numbers in parentheses are pure statistical errors (1σ level).

py, the fact that most of the Auger lines corresponds to one initial and one final state, makes it possible to have a deep insight into both the collision mechanism and the ionic structure.

From the point of view of the collision mechanism our conclusions can be summarized as follows. Information extracted from the measured vacancy-configuration distributions does not show any significant difference from the predictions of the independent-particle model. There are differences, higher than the statistical error, between the measured and fitted vacancy distributions, but we cannot find any tendency in it. The shapes of the measured and fitted distributions are practically identical even for the smaller members of them.

We found that the geometrical model of ionization[24] is quite good for strongly ionizing collisions (Ne and Ar
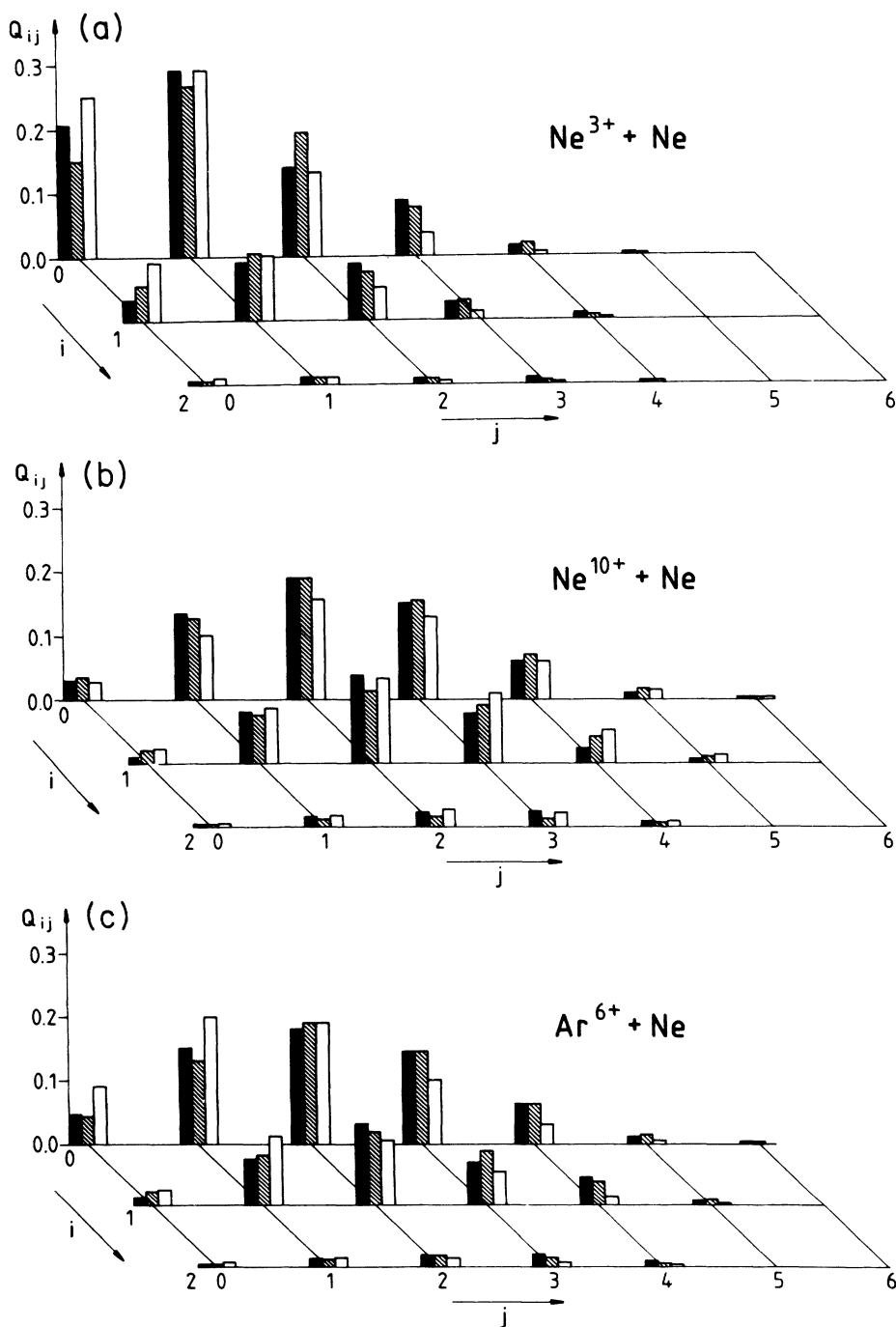
FIG. 3. Experimentally determined vacancy configurations (black bars; for their estimated uncertainty see Table IX) compared to the double binomial distributions fitted to the experimental data (shadowed bars) and to the theory (Ref. 24) (empty bars). i and j are the number of $2s$ and $2p$ vacancies.

projectiles) but it breaks down for the proton bombardment case where the interaction in the collision is the weakest one. For small probability values the geometrical model is supposed to underestimate the ionization and vacancy production probabilities for the outermost subshell because it does not take into account shake-off and shake-up processes.

Investigating the two-dimensional vacancy-configuration distributions we could not find any significant tendency in the ionization probabilities as a function of the degree of ionization, i.e., as a function of the increasing energy transfer which is necessary to eject more than one electron. This statement is not too strong,
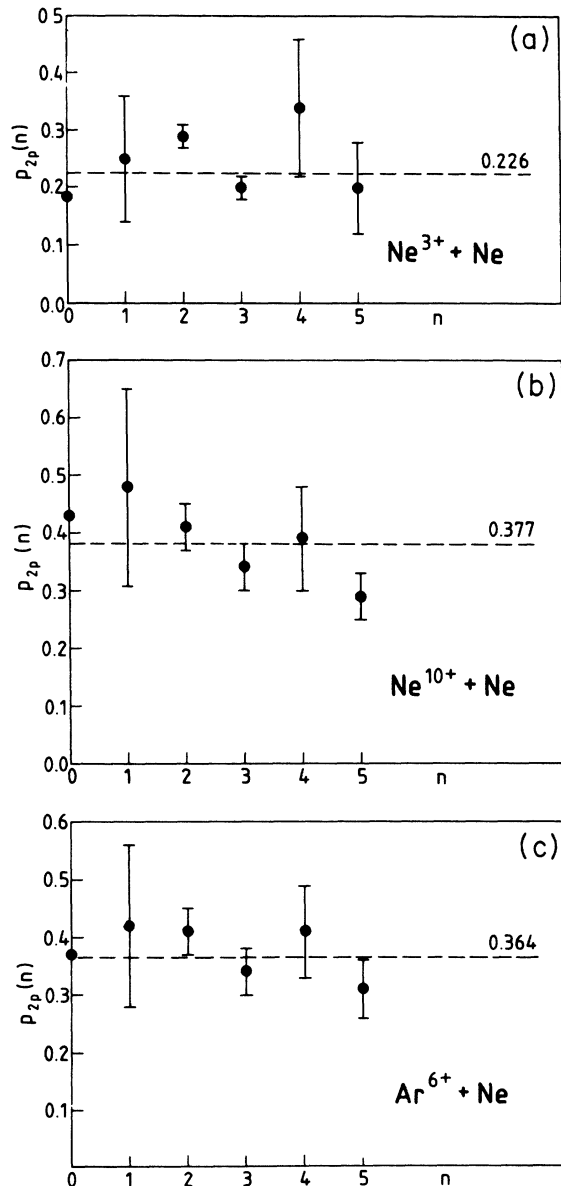
FIG. 4. p_{2p} as a function of the number of L vacancies n, calculated from the i,jth and $i,j + 1$th members of the experimentally determined distributions by using Eq. (9) and averaging over the i,j pairs for $n = i + j$ cases. The error bars show the scatter of the data of different i,j pairs.

however, because of the evidence of occurring improper branching ratios, initial-state weighting factors, and erroneous identifications. Anyhow, it is clear from our data that in the case of nearly-zero impact-parameter collisions concerned here one cannot find strong dependence of the ionization probabilities as a function of the degree of multiple ionization. This behavior may suggest the picture that mainly the distant collision region should be sensitive on the increased binding energies.

On the spectroscopic side the Auger transition energies, line intensities, and partly the angular distribution of the transitions were analyzed. A good agreement has been found between the experimental and theoretical Auger transition energies in Tables I and V–VII, where higher-order corrections (configuration mixing, relativistic and QED corrections, etc.) were involved in the calculations. Table II–IV, where only single configuration Dirac-Fock calculations in the LS coupling scheme are available for comparison, show much poorer agreement. This fact definitely suggests that higher-order corrections are not negligible in the theoretical calculations even in the case of low atomic numbers.

Similar conclusions can be derived for Auger transition rates. The theoretical calculations of Kelly[42] (Table I), in which higher-order corrections are involved, show very good agreement with experiment. However, there are only simpler calculations[43,44] for the multiple-ionized neon ion. It is the probable reason of the significant discrepancies between experimental and theoretical line intensity ratios in Tables II–VII.

The above conclusions are also supported by our angular distribution data. The $1s^12s^22p^5 \, ^1P - 1s^22s^22p^3 \, ^2P$ transition has a definitely anisotropic angular distribution.[20,21,40,41] This line should be strictly isotropic in the LS coupling scheme and without taking into account the configuration mixing.

Finally, it was pointed out, by analyzing the Auger line shapes, that the collision and deexcitation processes could not be completely separated from each other even for the high impact velocity region of the present study. A definite post-collision interaction was found between the ejected electrons and the deexciting ionic core in the cases of prompt Auger transitions.[31] While the energy spectrum of the ejected electrons has a strong soft part for even extremely high impact energies, the above finding may be a warning that separated collisional models and ionic structure calculations should be handled with care in the whole impact velocity region.

ACKNOWLEDGMENTS

[1]D. L. Matthews, in *Atomic Physics—Accelerators,* Vol. 17 of *Methods of Experimental Physics,* edited by P. Richard (Academic, New York, 1980), p. 433.

[2]D. Berényi, Adv. Electron. Electron Phys. **56**, 411 (1981).

[3]D. Berényi, in *Proceedings of the X84 International Conference on X-Ray and Inner-Shell Processes in Atoms, Molecules and Solids, Leipzig, German Democratic Republic, 1984,* edited by A. Meisel and J. Finster (Karl-Marx-Universität, Leipzig, 1984), p. 207.

[4]N. Stolterfoht, Phys. Rep. **146**, 315 (1987).

[5]N. Stolterfoht, in *Proceedings of the 3rd Workshop on High-energy in Ion-Atom Collisions, Debrecen, Hungary, 1987,* edited by D. Berényi and G. Hock (Springer-Verlag, Berlin, 1988), p. 3.

[6]D. Berényi, in *X-Ray Spectroscopy in Atomic and Solid State Physics,* Vol. 187 of *NATO Advanced Study Institute, Series B: Physics,* edited by J. Gomes Ferreira and M. Teresa Ramos (Plenum, New York, 1988), p. 25.

[7]C. F. Moore, J. J. Mackey, L. E. Smith, J. Bolger, B. M. Johnson, and D. L. Matthews, J. Phys. B **7**, L302 (1974).

[8]D. Schneider, C. F. Moore, and B. M. Johnson, J. Phys. B **9**, L153 (1976).

[9]N. Stolterfoht, D. Schneider, R. Mann, and F. Folkmann, J. Phys. B **10**, L281 (1977).

[10]D. L. Matthews, B. M. Johnson, J. J. Mackey, and C. F. Moore, Phys. Rev. Lett. **31**, 1331 (1973); D. L. Matthews, B. M. Johnson, J. J. Mackey, L. E. Smith, W. Hodge, and C. F. Moore, Phys. Rev. A **10**, 1177 (1974).

[11]R. Mann, F. Folkmann, and F. Beyer, J. Phys. B **14**, 1161 (1981).

[12]D. Schneider, M. Prost, B. DuBois, and N. Stolterfoht, Phys. Rev. A **25**, 3102 (1982).

[13]I. Kádár, S. Ricz, V. A. Shchegolev, B. Sulik, D. Varga, J. Végh, D. Berényi, and G. Hock, J. Phys. B **18**, 275 (1985).

[14]A. Itoh, T. Schneider, G. Schiwietz, Z. Roller, H. Platten, G. Nolte, D. Schneider, and N. Stolterfoht, J. Phys. B **16**, 3965 (1983).

[15]A. Itoh, D. Schneider, T. Schneider, T. J. M. Zouros, G. Nolte, G. Schiwietz, W. Zeitz, and N. Stolterfoht, Phys. Rev. **31**, 684 (1985).

[16]R. Bruch, N. Stolterfoht, S. Datz, P. D. Miller, P. L. Pepmiller, Y. Yamazaki, H. F. Krause, J. K. Swenson, K. T. Chung, and B. F. Davis, Phys. Rev. A **35**, 4114 (1987).

[17]N. Stolterfoht, P. D. Miller, H. F. Krause, Y. Yamazaki, J. K. Swenson, R. Bruch, P. F. Dittner, P. L. Pepmiller, and S. Datz, Nucl. Instrum. Methods B **24/25**, 168 (1987).

[18]S. Ricz, I. Kádár, D. Varga, J. Végh, T. Borbély, V. A. Shchegolev, D. Berényi, G. Hock, and B. Sulik, in *Proceedings of the 2nd Workshop on High Energy Ion-Atom Collisions, Debrecen, Hungary, 1984,* edited by D. Berényi and G. Hock (Akadémiai Kiadó, Budapest, 1985), p. 171.

[19]I. Kádár, S. Ricz, V. A. Shchegolev, D. Varga, J. Végh, D. Berényi, G. Hock, and B. Sulik, Phys. Lett. A **115**, 439 (1986).

[20]S. Ricz, I. Kádár, V. A. Shchegolev, D. Varga, J. Végh, D. Berényi, G. Hock, and B. Sulik, J. Phys. B **19**, L411 (1986).

[21]S. Ricz, J. Végh, I. Kádár, B. Sulik, D. Varga, D. Berényi, in *Proceedings of the 3rd Workshop on High-Energy Ion-Atom Collisions, Hungary, 1987,* edited by D. Berényi and G. Hock (Springer Verlag, Berlin, 1988), p. 197.

[22]I. Kádár, S. Ricz, B. Sulik, D. Varga, J. Végh, and D. Berényi, in *Proceedings of the 3rd Workshop on High-Energy Ion-Atom Collisions, Debrecen, Hungary, 1987,* edited by D. Berényi and G. Hock (Springer Verlag, Berlin, 1988), p. 479.

[23]I. Kádár, S. Ricz, D. Varga, B. Sulik, J. Végh and D. Berényi, J. Phys. (Paris) Colloq. **48**, C9-285 (1987).

[24]B. Sulik, I. Kádár, S. Ricz, D. Varga, J. Végh, G. Hock, and D. Berényi, Nucl. Instrum. Methods B **28**, 509 (1987); B. Sulik, G. Hock, and D. Berényi, J. Phys. B **17**, 3239 (1984); B. Sulik and G. Hock, in *Proceedings of the 2nd Workshop on High Energy Ion-Atom Collisions, Debrecen, Hungary, 1984,* edited by D. Berényi and G. Hock (Akadémiai Kiadó, Budapest, 1985), p. 183.

[25]I. Kádár, S. Ricz, B. Sulik, D. Varga, J. Végh, and D. Berényi, Nucl. Instrum. Methods B**40/41**, 60 (1989).

[26]Á. Kövér, D. Varga, Gy. Szabó, D. Berényi, I Kádár, J. Végh, and G. Hock, J. Phys. B **16**, 1017 (1983).

[27]D. Varga, J. Végh, Á. Kövér, S. Ricz, and A. Domonyi, Atomki Bull. **23**, 40 (1981); I. Kádár, B. Sulik, I. Cserny, T. Lakatos, and J. Végh, *ibid.* **23**, 42 (1981).

[28]L. Petterson, J. Nordgren, L. Selander, C. Nordling, and K. Siegbahn, J. Electron Spectrosc. Relat. Phenom. **27**, 29 (1982).

[29]I. Kádár, D. Berényi, S. Ricz, B. Sulik, D. Varga, and J. Végh, in *Spectroscopy and Collisions of Few-Electron Ions,* Proceedings of the Study Conference SCOFEI'88, Bucharest, Romania, 1988, edited by M. Ivascu, Viorica Florescu, and V. Zoran (World Scientific, Singapore, 1989), p. 434.

[30]J. Végh, I. Kádár, S. Ricz, B. Sulik, D. Varga, and G. Székely, Nucl. Instrum. Methods A **281**, 605 (1989).

[31]S. Ricz, I. Kádár, and J. Végh, Nucl. Instrum. Methods B**40/41**, 77 (1989).

[32]A. Niehaus and C. J. Zwakhals, J. Phys. B **16**, L135 (1983).

[33]M. O. Krause and J. H. Oliver, J. Phys. Chem. Ref. Data **8**, 329 (1979).

[34]R. Fletcher, Comput. J. **13**, 317 (1970).

[35]M. O. Krause, T. A. Carlson, and W. E. Moddeman, J. Phys. (Paris) Colloq. **32**, C4-139 (1971).

[36]D. L. Matthews, B. M. Johnson, and C. F. Moore, At. Nucl. Data Tables **15**, 41 (1975).

[37]R. J. Maurer and R. L. Watson, At. Nucl. Data Tables **34**, 185 (1986).

[38]S. Schumann, K. O. Groeneveld, and G. Nolte, Z. Phys. A **289**, 245 (1979).

[39]C. E. Moore, *Atomic Energy Levels,* Natl. Bur. Stand. (U.S.) Circ. No. 467 (U.S. GPO, Washington, DC, 1949), Vol. I.

[40]S. Ricz, I. Kádár, D. Varga, J. Végh, T. Borbély, and V. A. Shchegolev (unpublished).

[41]S. Ricz, G. Hock, I. Kádár, B. Sulik, D. Varga, J. Végh, and D. Berényi (unpublished).

[42]H. P. Kelly, Phys. Rev. A **11**, 556 (1975).

[43]C. P. Bhalla, J. Electron Spectrosc. Relat. Phenom. **7**, 287 (1975).

[44]M. H. Chen and B. Craseman, At. Data Nucl. Data Tables **38**, 381 (1988); M. H. Chen, Phys. Rev. A **31**, 1449 (1985).

[45]R. L. Becker, A. L. Ford, and J. F. Reading, Nucl. Instrum. Methods B **3**, 43 (1984); Phys. Rev. A **29**, 3111 (1984); Nucl. Instrum. Methods B**10/11**, 1 (1985).

[46]J. M. McGuire and P. Richard, Phys. Rev. A **8**, 1374 (1973).

[47]R. L. Kauffman, C. W. Woods, K. A. Jamison, and P. Richard, Phys. Rev. A **11**, 872 (1975).

[48]M. H. Chen and B. Craseman, Phys. Rev. A **12**, 959 (1975).

[49]G. Hock, B. Sulik, J. Végh, I. Kádár, S. Ricz, and D. Varga, Nucl. Instrum. Methods A **240**, 475 (1985).

[50]M. Horbatsch and R. M. Dreizler, Z. Phys. D **2**, 183 (1986); J. Ullrich, M. Horbatsch, V. Dagendorf, S. Kelbch, and H. Schmidt-Böcking, J. Phys. B **21**, 611 (1988).